Int. J. Electrochem. Sci., 6 **(2011)** 6653 - 6661

International Journal of
ELECTROCHEMICAL
SCIENCE
www.electrochemsci.org

An optimized Mn-doped $LiFePO_4$/C Composite Synthesized by Carbonthermal Reduction Technique

Ying Lin, Yingbin Lin[*], *Baozhi Zeng, Guiying Zhao, Ting Zhou, Meiling Chen, Xiamei Mao, Heng Lai, Zhigao Huang*[**]

Department of Physics, Fujian Normal University, Fuzhou 350007, China
[*]E-mail: yblin@fjnu.edu.cn; [**]E-mail:zghuang@fjnu.edu.cn

Received: 6 October 2011 / *Accepted:* 15 November 2011 / *Published:* 1 December 2011

Mn-doped $LiFePO_4$/C cathode materials were synthesized by a carbothermal reduction technique using sucrose as both the reduction agent and the carbon source. The microstructure and electrochemical performance were systematically investigated by X-ray diffraction (XRD), scanning electron microscopy (SEM), Raman spectroscopy, charge-discharge cycling, cyclic voltammograms and electrochemical impedance spectroscopy. It is found that the all as-prepared composites have a single phase of orthorhombic olivine-type structure and Mn^{2+} has successfully introduced into the M_2(Fe) sites. Among the as-prepared comosites, $LiFe_{0.98}Mn_{0.02}PO_4$/C demonstrates a best electrochemical property in terms of discharge capacity, electrochemical reversibility and cycling performance with an initial discharge capacity of 165 $mAh \cdot g^{-1}$ at a discharge rate of 0.2C. The improved electrochemical performance should be attributed to the smaller particle, the enhancement of the P-O bond and the facilitation of Li^+ ion "effective" diffusion induced by Mn^{2+}-substitution.

Keywords: Lithium-ion battery; $LiFePO_4$/C; Mn doping; Cycle performance

1. INTRODUCTION

Recently, phosphate-based materials have been studied intensively as a promising new class of cathode materials for lithium ion batteries because of their high stabilities. Among them olivine-structured $LiFePO_4$ is in the center of research due to its low cost, environmental benign, high and flat voltage profile (~3.4V versus Li/Li^+) and thermal stability[1-5]. However, $LiFePO_4$ suffers from poor high-rate capacity due to the low intrinsic electronic conductivity and poor lithium-ion diffusion [5-7]. Several strategies have been devised to overcome the inherent limitations of $LiFePO_4$, including the particle fining [8, 9], creating conductive coating (carbon or metal et al.) on the particles [10, 11], and doping with alien ion [12-15]. Fe-site doping is considered to be an effective way to improve the rate

performance of $LiFePO_4$, resulting from the increased the ionic mobility and diffusion coeffeicient. Sun et al. [13] proposed that the rate capability of $LiFePO_4$ was significantly enhanced by doping V. Ge et al. [14] reported that Ni doped $LiFePO_4$/C nanocomposite delivers high capacity up to 150 $mAh \cdot g^{-1}$ at 15C, retaining 93% after 7200 cycles. Many researches found that the electrochemical activity of Mn could be greatly improved in $LiFe_{1-x}Mn_xPO_4$ [16, 17]. In spite of the relative high potential of Mn^{2+}/Mn^{3+} redox couple and high energy density, the poor kinetics and large lattice distortion in olivine composites at high Mn content [18-20]. Furthermore, the two-plateau discharge profiles in Mn^{2+} heavily doped $LiFe_{1-x}Mn_xPO_4$ may hinder its practical application. In present work, the effect of the partial substitution of Fe^{2+} with Mn^{2+} at low content on the electrochemical performance have been systematically investigated from the viewpoint of the lithium ion diffusion.

2. EXPERIMENTAL

Olivine structured $LiFe_{1-x}Mn_xPO_4$/C (x=0.00, 0.02, 0.05, 0.10) composites were prepared by a carbothermal reduction method. Amount of $CH_3COOLi \cdot 2H_2O$, $FeC_2O_4 \cdot 2H_2O$, $NH_3H_2PO_4$ and MnO_2 (analytical reagent) as precursor materials were mixed in a stoichimetric ratio ($n_{Li} : n_{Fe} : n_{Mn} : n_p = 1 : 1\text{-}x : x : 1$) and sucrose ($C_{12}H_{22}O_{11}$) was added as carbon source.

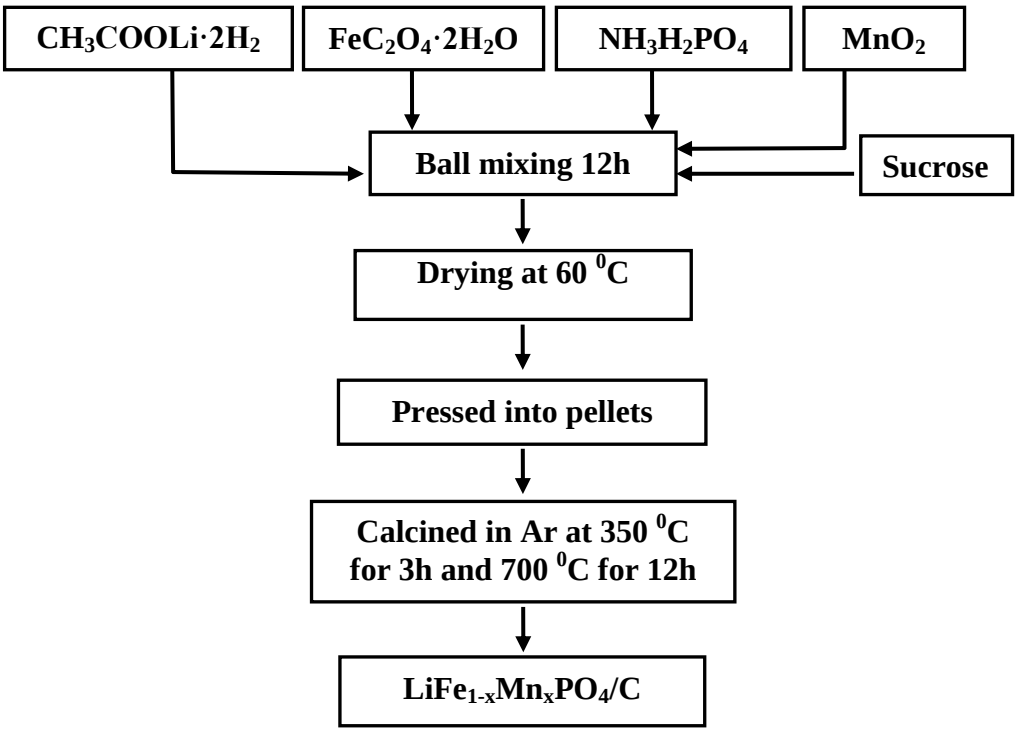

Figure 1. Flow chart for preparation of $LiFe_{1-x}Mn_xPO_4$/C composites.

First, the mixture were planetary milled in ethanol phase for 12h and subsequently dried at 60 ℃ in an oven. The resulting precursor was calcined at 350℃ for 3h and subsequently sintered at 700℃ for 12h in an inert atmosphere. The flow chart of the preparation of $LiFe_{1-x}Mn_xPO_4/C$ composites is shown in Fig. 1. The microstructures of pristine and Mn-doped $LiFePO_4/C$ were characterized with XRD with a Cu Kα radiation, scanning electron microscope (JEOL JSM-7500) (SEM) and Raman spectra.

The work electrodes were prepared by homogeneously pasting slurry containing 80wt.% $LiFe_{1-x}Mn_xPO_4/C$, 10wt.% super-P and 10wt.% polyvinylidene fluoride (PVDF) dissolved in N-methylpyrolline onto an aluminum foil and dried in a vacuum oven at 110℃ for 12h. The obtained sheets were punched into circular strips of 12.5mm in diameter, and about 3.0mgcm^{-2} active material was loaded on an Al foil. Before use, the work sheets were pressed at 3 Mpa and subsequently dried in vacuum at 80℃ for 5h to avoid possible water contamination. The coin cells (CR 2025) were assembled in an argon-filled glove box using a metal lithium foil as reference electrode, Celgard 2300 microporous polyethylene membrane as the separator and 1M LiPF6 in a mixture of ethyl carbonate (EC) and dimethyl carbonate (DMC) (1:1 in vol. ratio) as the electrolyte. The cells were galvanostatically charged and discharged between 2.5 and 4.3V versus Li^+/Li under a Land CT2001 Battery Tester at room temperature. Cyclic voltammograms (CV) were performed for both pristine and Mn-doped $LiFePO_4/C$ composite at a scan rate of $0.1mV \cdot s^{-1}$ between 2.5-4.3V. The electrochemical impedance measurements were carried out using CHI660C electrochemical work station with applied 10 mV sinusoidal perturbation in a frequency range from 100 KHz to 0.01Hz at room temperature.

3. RESULTS AND DISCUSSION

Fig.2 shows the XRD patterns of the as-prepared $LiFe_{1-x}Mn_xPO_4/C$ composites.

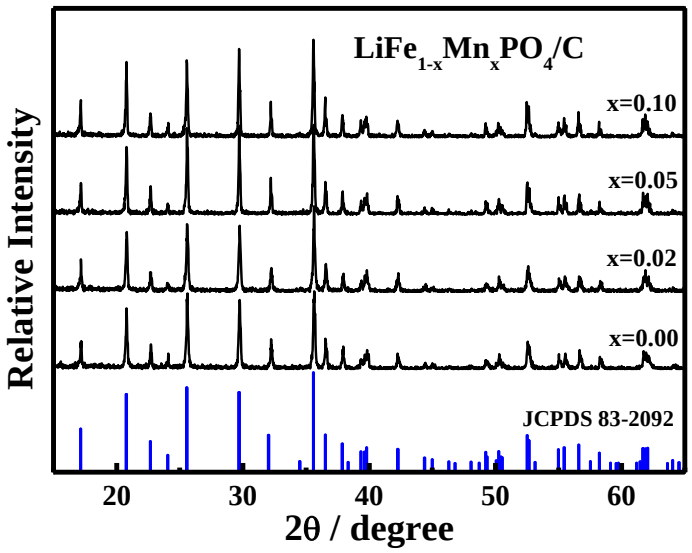

Figure 2. XRD patterns of $LiFe_{1-x}Mn_xPO_4/C$ (x=0.00, 0.02, 0.05, 0.10) powders.

Table 1. Calculated lattice parameters of $LiFe_{1-x}Mn_xPO_4/C$ (x=0.00, 0.02, 0.05, 0.10) powders.

Lattice parameter	Samples			
	$LiFePO_4/C$	$LiFe_{0.98}Mn_{0.02}PO_4/C$	$LiFe_{0.95}Mn_{0.05}PO_4/C$	$LiFe_{0.9}Mn_{0.1}PO_4/C$
a ($\overset{o}{A}$)	10.3148	10.3237	10.3319	10.3335
b ($\overset{o}{A}$)	6.0049	6.0070	6.0087	6.0147
c ($\overset{o}{A}$)	4.6901	4.6867	4.6878	4.6898
Volume of unit ($\overset{o}{A}^3$)	290.50	290.64	291.02	291.48

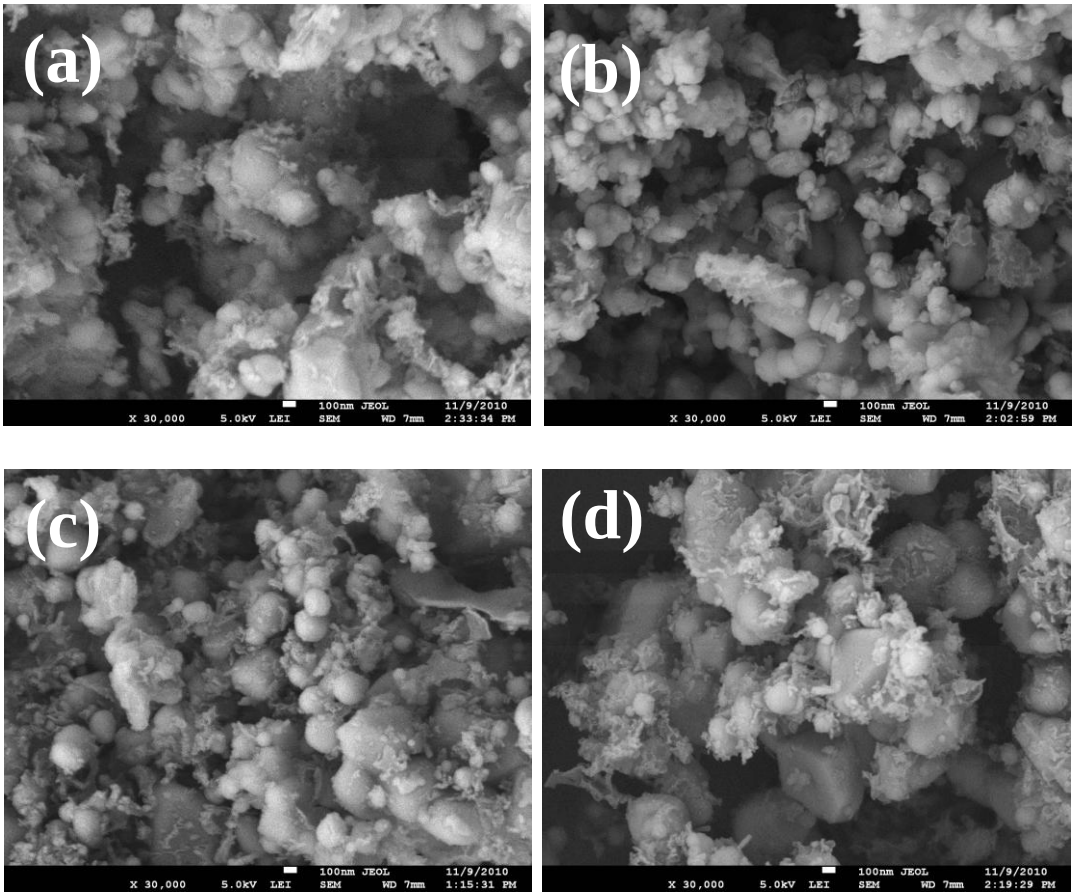

Figure 3. SEM images of as-prepared (a) $LiFePO_4/C$, (b) $LiFe_{0.98}Mn_{0.02}PO_4/C$, (c) $LiFe_{0.95}Mn_{0.05}PO_4/C$ and (d) $LiFe_{0.9}Mn_{0.1}PO_4/C$.

It is found that Mn-doped $LiFePO_4/C$ is well crystallized in orthorhombic structure as the pristine one without any unexpected phase, such as Fe_2P or Mn-containing compound [21]. The lattice constants of these composites were calculated based on the XRD patterns and are listed in Table 1. Compared with the pristine $LiFePO_4/C$, Mn-doping results in slight expansion of *a*-axis and cell volume, indicating that Mn^{2+} has successfully introduced into the M_2 (Fe) sites because the ionic radius of Mn^{2+} (0.083nm) is larger than that of Fe^{2+} (0.078nm). The expansion in cell volume is expected to

provide more space for lithium intercalation/de-intercalation [22]. The typical scanning electron micrographs of as-prepared pristine and Mn-doped $LiFePO_4$/C composites are presented in Fig. 3. It shows that they are consisted of non-uniform fine particles with the size ranged between 100nm and 400nm, and the conducting carbon is uniformly distributed in composites. The $LiFe_{0.98}Mn_{0.02}PO_4$/C particles was much smaller size and more dispersive than that for other samples.

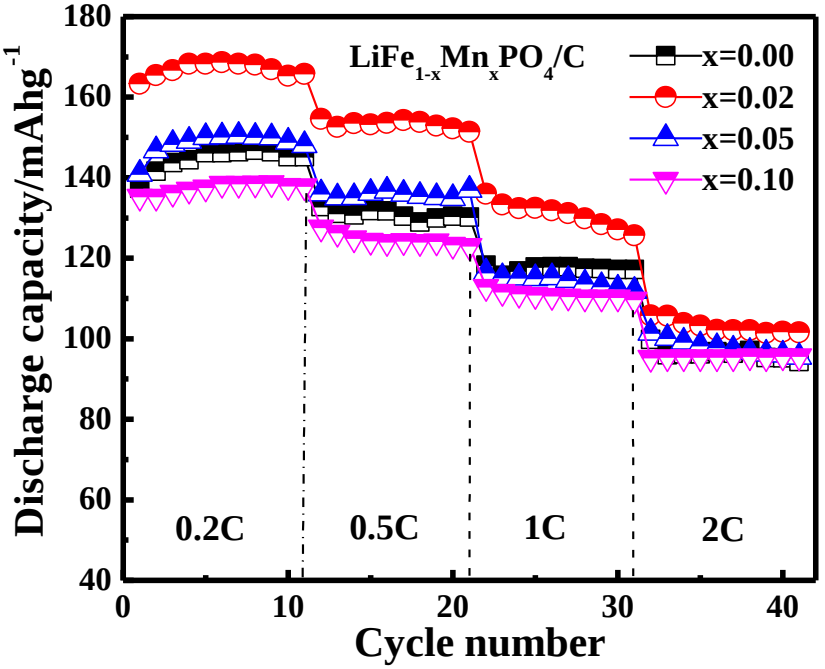

Figure 4. Cycling performances of $LiFe_{1-x}Mn_xPO_4$/C (x=0.00, 0.02, 0.05, 0.10) cathodes with different rates in the voltage range of 2.5-4.3V.

Fig.4 shows the galvanostatic charge/discharge curves of pristine and Mn-doped $LiFePO_4$/C cathodes, which were operated at different current densities in the voltage range of 2.5 – 4.3 V(*vs.* Li^+/Li). The charge-discharge processes of the samples are taken for 10 cycles at the rates of 0.2 C (1C= 170 $mAh \cdot g^{-1}$), 0.5 C, 1.0 C and 2.0 C, respectively. It is also found that $LiFe_{0.98}Mn_{0.02}PO_4$/C exhibits the best cycling performance with the highest discharge capacities of 165, 152, 131 and 102$mAh \cdot g^{-1}$ at the rates of 0.2C, 0.5C, 1C and 2C, respectively. In contrast, the pristine one delivers only 146, 130, 118 and 98 $mAh \cdot g^{-1}$, respectively. The improved cycling performance of $LiFe_{0.98}Mn_{0.02}PO_4$/C may be mainly ascribed to the smallest particle-size as well as the uniform size distribution. Size reduction of $LiFePO_4$ would shorten electronic conduction path and consequently facilitate the intercalation process of lithium ions, resulting in improve the charge and discharge kinetic [23-26]. On the other hand, Mn^{2+}-substitution may induce Li^+ defect in $LiFePO_4$ and residue of Fe^{2+}/Fe^{3+} coexistence state due to the balance of electrical valence. Such defects are favorable for the diffusion of Li^+ in solid phase and enhance electrical conductivity. As a result, high discharge capacity and good reversibility were obtained.

Fig.5 shows the Raman spectra of $LiFePO_4/C$ and $LiFe_{0.98}Mn_{0.02}PO_4/C$ composites, dominated by the stretching and bending vibration modes of PO_4^{3-} ions.

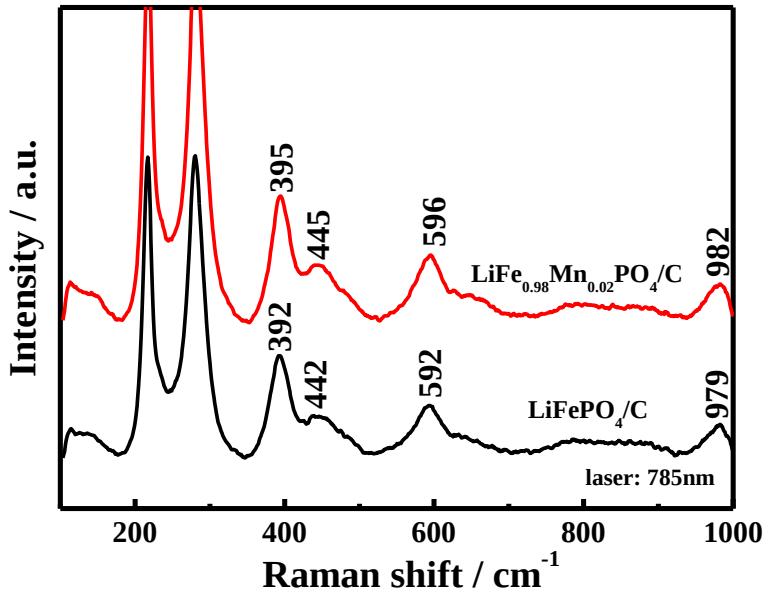

Figure 5. Raman spectrum of $LiFePO_4/C$ and $LiFe_{0.98}Mn_{0.02}PO_4/C$ composites.

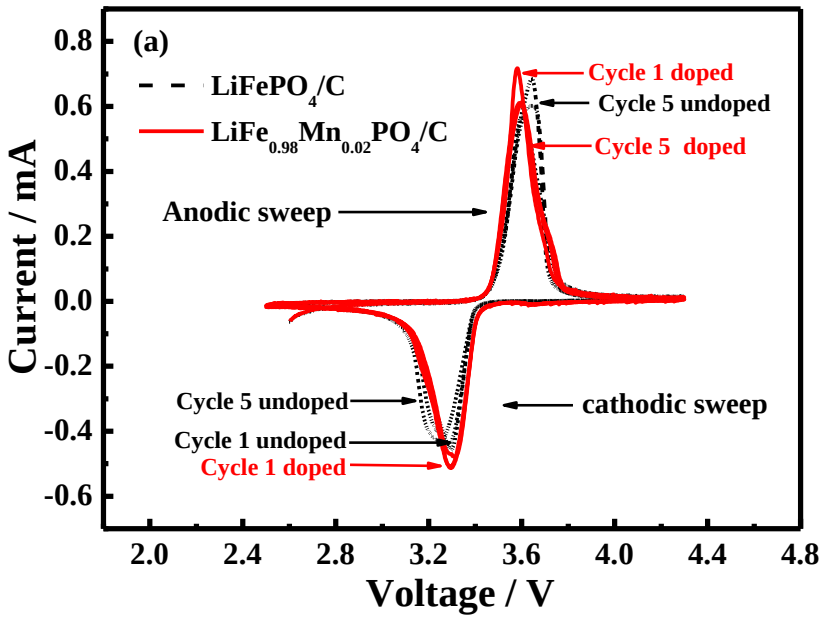

Figure 6. (a) Cyclic voltammograms of the $LiFePO_4/C$ and $LiFe_{0.98}Mn_{0.02}PO_4/C$ electrodes at a scan rate of $0.1mV \cdot S^{-1}$; (b) Electrochemical impedance spectra of the $LiFePO_4/C$ and $LiFe_{0.98}Mn_{0.02}PO_4/C$ electrodes. Inset of (b) is the equivalent circuit established for the simulation of impedance spectra.

The Raman peaks located around the ranges of 970, 390 and 596cm^{-1} are identified as the vibration of the P-O bond [19, 22]. In contrast, the Raman peaks of $LiFe_{0.98}Mn_{0.02}PO_4/C$ are shifted towards higher wavenumber than that of $LiFePO_4/C$ composite, indicating $LiFe_{0.98}Mn_{0.02}PO_4/C$ composite has a most stable structure of the lithium iron phosphate for the charge/discharge reaction.

To get insight into the kinetics of lithium intercalation/deintercalation, cyclic voltammetry (CV) and electrochemical impedance spectroscopy (EIS) were carried out at room temperature. Fig.6 (a) shows the CV curves of $LiFePO_4/C$ and $LiFe_{0.98}Mn_{0.02}PO_4/C$ composites at a scan rate of 0.1mV·s^{-1} in the 2.5-4.3V (*vs.* Li^+/Li). Both composites exhibit the anodic and cathodic peaks around 3.4V, corresponding to the two-phase charge–discharge reaction of the Fe^{2+}/Fe^{3+} redox couple [27, 28]. It can be found that $LiFe_{0.98}Mn_{0.02}PO_4/C$ demonstrates a better step in oxidation-reduction process than the pristine one and the polarization defined as potential difference between the anodic and the cathodic peaks is reduced with the Mn^{2+}-substitution. These behaviours tend to indicate that kinetic limitations on the electrochemical redox reaction were relaxed with the substitution [29, 30]. Furthermore, the integration of the area under the anodic and cathodic peaks suggests that an equal quantity of lithium ions might be reversibly de-inserted and re-inserted into $LiFe_{0.98}Mn_{0.02}PO_4/C$ composite during the charge-discharge cycling.

The typical Nyquist plots of the as-prepared pristine and $LiFe_{0.98}Mn_{0.02}PO_4/C$ electrodes after 50 cycles under 0.5C current density are shown in Fig. 6 (b). The overall shape of Nyquist plot is composed of a depressed semicircle in the high frequency region and an oblique straight inclined line in the low frequency region. The semicircle part at high frequencies is attributed to the lithium-ion transfer resistances at the interface between the cathode particles and an electrolyte [29] and the linear part at low frequencies is attributed to the diffusion of Li^+ in the $LiFePO_4$ electrode materials [31]. A simplified equivalent circuit model inset in Fig.6 (b) was employed to analyze the impedance spectra, where the symbols, R_s, R_{ct}, and Z_w, denoted the solution resistance, charge-transfer resistance and Warburg impedance, respectively. CPE is placed to represent the double layer capacitance and passivation film capacitance. Significant decrease of R_{ct} from 440.7Ω in $LiFePO_4/C$ to 253.1Ω in $LiFe_{0.98}Mn_{0.02}PO_4/C$ composite can be found, indicating the enhancement of the charge-transfer reaction of the $LiFePO_4/C$ with Mn^{2+}-substitution. Thus, the transportation of electrons was improved. Similar phenomena have been reported by other research groups [31, 32]. Nakamura found that partial substitution of Fe^{2+}/Mn^{2+} remarkably influenced both electronic and ionic conductivities in LiFePO4 series [32].

4. CONCLUSION

Substitution of iron with manganese in olivine-structure $LiFePO_4/C$ composite was successfully prepared through a carbothermal reduction technique. Analysis from XRD and SEM show that as-prepared composites are well crystallized in orthorhombic structure and cell volume as well as the morphology varies with the Mn^{2+} content. Among the as-prepared composites, $LiFe_{0.98}Mn_{0.02}PO_4/C$ composite shows the highest reversible capacity. Taking into account all the analyses and results presented above, it can be concluded that the enhancement of chemical performance with Mn^{2+}-

substitution is attributed to the optimization of the morphology, structure stability and ionic conductivities, which facilitate the Li^+ ion diffusion in composites.

ACKNOWLEDGEMENTS

This work was supported by a grant from National Science Foundation for Young Scholars （No. 11004032）and Natural Science Foundation of China (No.11074039)

References

1. Ji-S. Oh, S.-H. Kim, Y. Kang, D.-W. Kim, *J. Power Sources* 163 (2006) 229.
2. D. A. D. Aurbach, B. Markovsky, G. Salitra, E. Markevich, Y. Talyossef, M. Koltypin, L. Nazar, B. Ellis, D. Kovacheva, *J. Power Sources* 165 (2007) 491.
3. J. Q. Xu, H.R. Thomas, R. W. Francis, K. R. Lum, J. W. Wang, B. Liang, *J. Power Sources* 177 (2008) 512.
4. X. M. Wang, Y. Sone, H. Naito, C. Yamada, G. Segami, K. Kibe, *J. Power Sources* 161 (2006) 594.
5. D. Jugovi´c, D. Uskokovi´c, *J. Power Sources* 190 (2009) 538..
6. W. J. Zhang, *J. Power Sources* 196 (2011) 2964.
7. J. Molenda, W. Ojczyk, J. Marzec, *J. Power Sources* 174 (2007) 689-690.
8. Y. H. Huang, H. B. Ren, S. Y. Yin, Y. H. Wang, Z. H. Peng, Y. H. Zhou, *J. Power Sources* 195 (2010) 611.
9. D. Rangappa, K. Sone, T. Kudo, I. Honma, *J. Power Sources* 195 (2010) 6167.
10. C.H. Mi, Y.X. Cao, X.G. Zhang, X.B. Zhao, H.L. Li, *Powder Technol*. 181 (2008) 301.
11. B. Zhang, X. J. Wang, H. Li, X. J. Huang, *J. Power Sources* 189 (2009) 463.
12. X. Q. Ou, G. C. Liang, L. Wang, S. Z. Xu, X. Zhao, *J. Power Sources* 184 (2008) 543.
13. C.S. Sun, Z. Zhou, Z. G. Xu, D. G. Wang, J. P. Wei, X. K. Bian, J. Yan, *J. Power Sources* 193 (2009) 841.
14. Y. C. Ge, X. D. Yan, J. Liu, X. F. Zhang, J. W. Wang, X. G. He, R. S. Wang, H. M. Xie, *Electrochim. Acta* 55 (2010) 5886.
15. L. Wu, X. H. Li, Z. X. Wang, X. J. Wang, L. J. Li, J. Fang, F. X. Wu, H. J. Guo, *Powder Technol*. 199 (2010) 293.
16. A.Yamada, Y. Kudo, K.Y. Liu, *J. Electrochem. Soc*., 148 (2001) A747.
17. G. H. Li, H. Azuma, M. Tohda, *J. Electrochem. Soc*., 149 (2002) A743.
18. J. K. Kim, G. S. Chauhan, J. H. Ahn, H. J. Ahn, *J. Power Sources* 189 (2009) 391.
19. M. Bini, M. C. Mozzati, P. Galinetto, D. Capsoni, S. Ferrari, M. S. Grandi, V. Massarotti, *J. Solid State Chem*. 182 (2009) 1972.
20. The Nam Long Doan, Izumi Taniguchi, *J. Power Sources* 196 (2011) 1399.
21. Y. Feng, Mater. Chem. Phys. 121 (2010) 305.
22. Y. Lu, J. C. Shi, Z. P. Guo, Q. S. Tong, W. J. Huang, B. Y. Li, *J. Power Sources* 194 (2009) 788.
23. P. S. Herle, B. Ellis, N. Coombs, L. F. Nazar, *Nat. Mater*. 3 (2004) 147.
24. C. Delacourt, P. Poizot, M.Morcrette, J. M. Tarascon, C. Masquelier, *Chem. Mater*. 16 (2004) 93.
25. L. J. Li, X. H. Li, Z. X. Wang, L. Wu, J. C. Zheng, H. J. Guo, *J. Phys. Chem. Solids* 70 (2009) 240.
26. P. Gibot,M. C. Cabanas, L. Laffont, S. Levasseur, P. Carlach, S. Hamelet, J. M. Tarascon, C. Masquelier,. *Nat. Mater*. 7 (2008) 741.
27. H. C. Kang, D. K. Jun, B. Jin, E. M. Jin, K. H. Park, H. B. Gu, K. W. Kim, *J. Power Sources* 179 (2008) 342.
28. X. Z. Liao, Z. F. Ma, Q. Gong, Y. S. He, L. Pei, L. J. Zeng, *Ectrochem. Commun*. 10 (2008) 692.
29. X. G. Yin, K. L. Huang, S. Q. Liu, H. Y. Wang, H. Wang, *J. Power Sources* 195 (2010) 4312.

30. C. S. Sun, Y. Zhang, X. J. Zhang, Z. Zhou, *J. Power Sources* 195 (2010) 3682.
31. W. K. Zhang, Y. L. Hu, X. Y. Tao, H. Huang, Y. P. Gan, C. T. Wang, *J. Phys. Chem. Solids* 71 (2010) 1199.
32. T. Nakamura, K. Sakumoto, M. Okamoto, S. Seki, Y. Kobayashi, T. Takeuchi, M. Tabuchi, Y. Yamada, *J. Power Sources* 174 (2007) 435.